Combustion and Flame 174 (2016) 179–193

Contents lists available at ScienceDirect

Combustion and Flame

journal homepage: www.elsevier.com/locate/combustflame

The role of low temperature chemistry in combustion mode development under elevated pressures

Jiaying Pan[a], Haiqiao Wei[a,*], Gequn Shu[a], Zheng Chen[b], Peng Zhao[c,*]

[a] State Key Laboratory of Engines, Tianjin University, Tianjin 300072, China
[b] SKLTCS, Department of Mechanics and Engineering Science, Peking University, Beijing 100871, China
[c] Department of Mechanical Engineering, Oakland University, Rochester, MI 48309, USA

ARTICLE INFO

Article history:
Received 4 May 2016
Revised 20 June 2016
Accepted 9 September 2016

Keywords:
Negative Temperature Coefficient (NTC)
Auto-ignition
Cool flame
Spontaneous propagation
Livengood–Wu integral
Knocking intensity

ABSTRACT

Negative Temperature Coefficient (NTC) behavior is an essential feature of low-temperature oxidation for large hydrocarbon fuels, which is of particular relevance to cool flame and auto-ignition. In this study, using n-heptane as a typical fuel exhibiting NTC, combustion phenomena involving both auto-ignition and flame propagation are computationally studied at initial temperatures within and above NTC regime under elevated pressures in a one-dimensional planar constant-volume configuration, with detailed kinetics and transport. Multi-staged flame structures representing cool flame and hot flame are observed, and consequently, different types of auto-ignition are identified during two-staged and single-staged flame propagation scenarios by varying initial temperature. Specially, as the initial temperature increases, the behavior of cool flame is gradually suppressed and auto-ignition position is transferred from the location ahead of flame front to end-wall region, leading to different combustion modes and peak pressure magnitudes. Moreover, attributed to the chemical reactivity processed by cool flame, the flame propagation of the cases within NTC regime is even faster than those beyond NTC regime. A recently developed two-staged Livengood–Wu integral is further utilized to predict these auto-ignition scenarios, yielding good agreement and further demonstrating the significant role of NTC chemistry in modifying the thermodynamic state and chemical reactivity at upstream of a reaction front. Finally, different combustion modes and knocking intensity for these detailed calculations are summarized in non-dimensional diagrams, which suggest that a higher initial temperature does not guarantee a higher knocking intensity, instead, the developing and developed detonation wave initiated by an auto-ignition occurring within NTC regime could even induce higher knocking intensity in comparison to the thermal explosion under the temperatures beyond NTC regime.

© 2016 The Combustion Institute. Published by Elsevier Inc. All rights reserved.

1. Introduction

Downsized spark-ignited (SI) engines have become increasingly attractive because of their high thermal efficiency and low CO_2 emissions. However, the risk of knock and super-knock has been a large obstacle especially for downsized engines operating under low-speed and high-load conditions [1]. It is generally considered that engine knock is caused by end-gas auto-ignition before the arrival of SI flame [2], while super-knock is attributed to a developing detonation resulting from a resonance between acoustic waves by auto-igniting hot-spots and a reaction wave propagating along negative temperature gradient in multi-scale turbulent flow field [3]. When super-knock occurs, the stochastic auto-igniting hot-spots may consume the entire mixture within less than a millisecond and thus cause a knocking intensity beyond 200 bar [4]. Despite the numerous studies devoted to engine knock and super-knock, due to the complex nature of the problem itself, there are still many ambiguities associated with the key physical-chemical mechanisms, such as reaction-pressure wave interactions [5,46,47], deflagration to detonation transition (DDT) [6,46] and the role of chemistry [7].

Addressing a thermal hot spot characterized by certain radius and temperature gradient in one-dimensional (1D) configuration, a pioneering work by Zel'dovich [8] proposed that there are three kinds of reaction wave front affected by auto-ignition, corresponding to supersonic auto-ignition, detonation and subsonic auto-ignition with different propagation speeds compared with speed of sound, respectively. In this classification, thermal explosion represents a limiting case of supersonic auto-ignition with an

---

* Corresponding authors.
E-mail addresses: whq@tju.edu.cn (H. Wei), pengzhao@oakland.edu, zhaodbustc@gmail.com (P. Zhao).

http://dx.doi.org/10.1016/j.combustflame.2016.09.012
0010-2180/© 2016 The Combustion Institute. Published by Elsevier Inc. All rights reserved.

infinite propagation speed of the reactive front. Based on Zel'dovich auto-ignition concept, Bradley and coworkers [9–13] showed that depending on initial temperature gradients within a hot spot, a quantitative diagram consisting of a normalized temperature gradient (ξ) and the ratio of acoustic time to excitation time of chemical energy release (ε) could be developed, which is capable of further classifying different auto-ignition modes with regime boundaries, including subsonic deflagrative auto-ignition, developing detonation, supersonic deflagrative auto-ignition and thermal explosion. Recently this diagram has been extensively utilized to analyze engine knock and super-knock [13,14]. Later, Rudloff et al. [15] introduced a third non-dimensional parameter (π), representing the conversion of chemical energy in end-gases into overpressure, to evaluate the efficiency of auto-ignition on knocking severity for pre-ignition in realistic engines. These methodologies basically provide quantitative criteria on abnormal combustion based on whether reaction front can couple with pressure wave or not. More recently, Grogan et al. [16] developed an ignition regime diagram with consideration of turbulence, chemistry and heat transfer in rapid compression machines. Im et al. [17] proposed non-dimensional criteria to predict weak and strong ignition regime of homogeneous reactant mixture with turbulence and temperature fluctuations. Therefore, turbulence has been further included to classify different auto-ignition regimes. However, these studies only consider simplified chemistry and/or simple fuels, without accounting for the essential features of the oxidation of large hydrocarbon fuels, such as low-temperature chemistry (LTC) and negative-temperature coefficient (NTC) phenomenon [18], which will fundamentally affect the auto-ignition kinetics and induce substantial non-monotonicity into combustion system. Meanwhile, according to the theoretical analysis on ignition delay gradient in [9], severe knock could be induced in NTC regime, while this point has not been adequately addressed using above non-dimensional analysis. Therefore, it merits more research on the potential effect of LTC on above combustion modes and their classifications.

NTC behavior is of significant relevance to engine knock in SI engines [19], cool flame [20], flame stabilization [21] and the combustion of homogeneous charge compression ignition (HCCI) engines [22]. Sun et al. [23] numerically investigated the transitions from ignition to flames as well as the combustion dynamics in stratified n-heptane/air mixture, which showed that the rich LTC reactivity with fuel stratification can lead to knocking and acoustic formation. Ju et al. [24] numerically investigated ignition and flame propagation in n-heptane/air mixture, and they found that there were at least six different combustion regimes at the temperatures near NTC. Martz et al. [25] analyzed the physical processes of auto-igniting end-gas influencing reaction front propagation under spark-assisted compression ignition (SACI) combustion conditions. However, the evolutions of flame propagation and pressure/shock waves induced by local auto-ignition were not considered. Chen and coworkers [26,27] identified different supersonic auto-ignition modes and reaction-pressure wave interactions caused by a cool spot in NTC regime for n-heptane/air mixture, with emphasis on the transient evolutions following an artificial thermal stratification as an initial condition, while the evolutions of flame propagation, auto-ignition and subsequent reaction front remain unclear. In addition, most previous studies have been focused on high-temperature conditions [28,29], but systematic studies are still needed for the conditions involving both hot and cool flames in NTC regime.

The primary objectives of current numerical investigation are to further explore the role of LTC on the interactions of flame propagation and auto-ignition, especially in NTC regime, to provide fundamental understandings for such physical–chemical processes and to gain practical insights for LTC effect on knocking combustion. As a major component of Primary Reference Fuel (PRF), n-heptane has been extensively studied with its chemistry relatively well understood and validated. Moreover, it qualitatively shares the same NTC chemistry pathways with other gasoline surrogates (e.g. iso-octane), despite its much lower octane index [5,26,30]. Actually, with the tendency of intake boost and engine downsizing, it is expected that NTC regime shall shift to high temperature region, leading to greater relevance of low temperature even for regular gasoline. Therefore, n-heptane is considered in current study as a representative fuel with NTC behavior. Meanwhile, the current work is based on a simplified constant-volume configuration with well-defined initial and boundary conditions, which allows detailed chemistry and transport and includes most of the essential physical and chemical components during knocking combustion, such as flow unsteadiness, hot-spot(s) auto-ignition, deflagration/detonation wave and pressure/shock wave propagation with little ambiguity in analysis.

2. Model validation and specifications

The skeletal mechanism for n-heptane oxidation adopted in current work is from Yoo et al. [31], which includes 88 species and 387 reactions, and it has been validated and tested against a wide range of combustion targets such as ignition delay time and laminar flame speed. Figure 1(a) shows the comparisons of ignition delay time of stoichiometric n-heptane/air calculated by three reaction mechanisms [31–33] under low and high pressure conditions, together with shock tube experimental data [34]. These results indicate that current mechanism is able to accurately predict low-to-high temperature ignition, including NTC regime. Meanwhile, the current mechanism has been validated against the laminar flame speed measurement at different pressures and equivalence ratios [35], yielding satisfactory agreement, as shown in Fig. 1(b). Another widely used kinetic model Jetsurf 1.0 [36], without low temperature chemistry, is also utilized to calculate the flame speed under the same conditions for comparison. The good agreement demonstrates the capability of both mechanisms in predicting regular laminar flame propagation and implies the insignificant role of low temperature chemistry on flame propagation with normal temperatures.

For laminar flame calculation with normal and elevated unburned temperatures, PREMIX [37] is utilized to calculate the 1D steady planar flame, which is further applied as initial condition of the unsteady simulation, where the flame front starts to propagate in the auto-ignitive mixture. An in-house code A-SURF (Adaptive Simulation of Unsteady Reactive Flow) is used to perform the simulations of unsteady reactive flow by solving full governing equations with detailed chemistry and mixture-averaged formulation of the detailed transport properties. During the simulations, the second-order, Strang splitting fractional-step procedure is adopted to separate the time evolution of stiff reaction term from that of the convection and diffusion terms. In the first step, the non-reactive flow is resolved and the second-order Runge–Kutta, MUSCL-Hancock and central difference schemes are employed to calculate temporal integration, convective and diffusion flux, respectively. The second step is to solve the chemistry term using the VODE solver [38]. A multi-level algorithm with dynamic adaptive mesh refinement has been used here, which can accurately resolve ignition initiation, reaction front and pressure/shock wave as well as detonation wave, as shown in previous work [39–41]. In current work, the finest mesh Δx is 0.8 μm, and minimum Courant–Friedrichs–Lewy (CFL) number is maintained to be less than 0.1 with corresponding time step $\Delta t = 5\times10^{-13}$ s, which can keep good stability and convergence during the whole computation. The detailed code specifications and validation can be further found in [39–41].

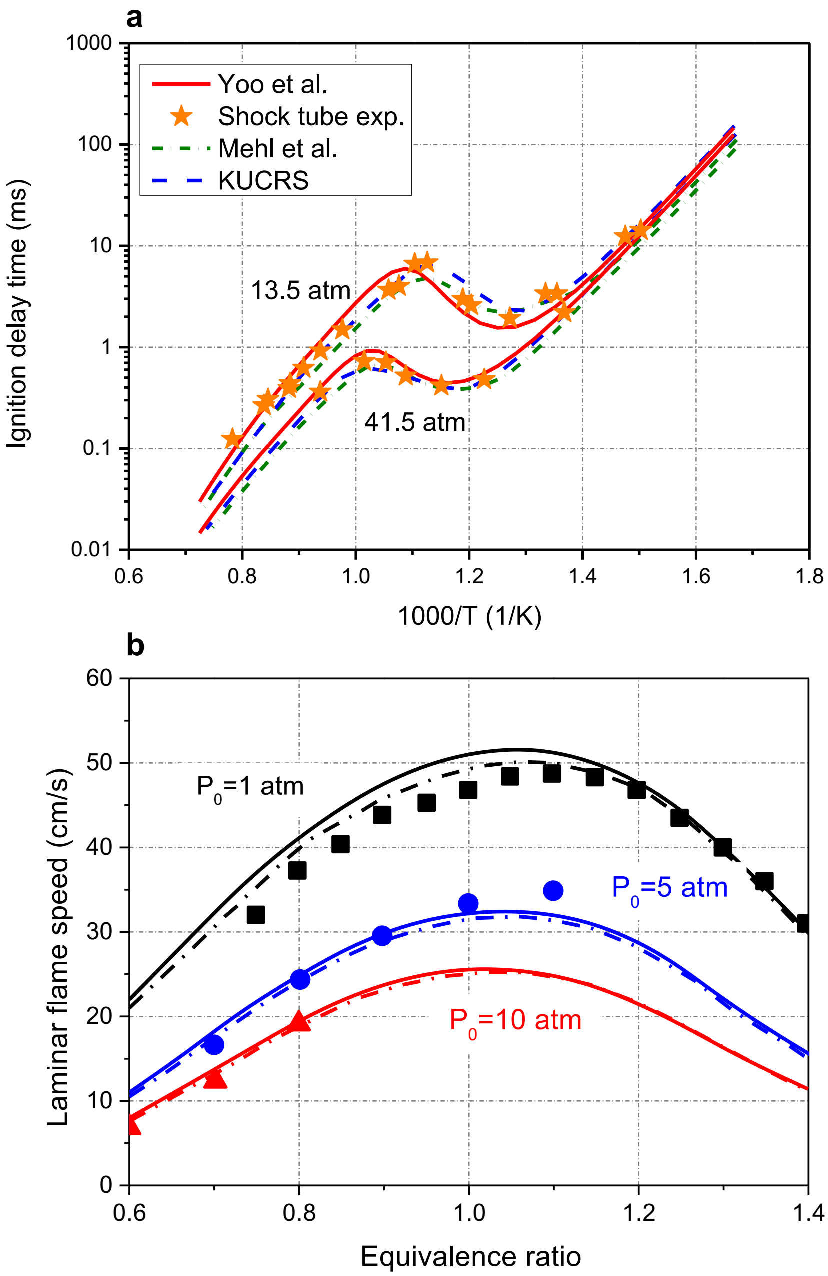

Fig. 1. (a) Ignition delay time for stoichiometric n-heptane/air mixture at adiabatic constant-volume conditions. (b) Comparisons of laminar flame speed between experiments (symbols) [35] and calculations at different equivalence ratios (Solid lines for JetSurF 1.0 [36], Dashed lines for current mechanism).

3. Results and discussion

3.1. NTC-affected flame propagation

It is expected with gradually elevated inlet temperature, the role of auto-ignition and NTC chemistry should be more significant on flame propagation. To demonstrate such effects, 1D steady premixed flame under $P_0 = 40$ atm is calculated for stoichiometric n-heptane/air mixture at different inlet temperatures from $T_{in} = 700$ to 1100 K, with temperature and heat release rate profile presented in Fig. 2, which is shown in a reference frame that is moving with the flame. It is observed that as T_{in} increases from 700 to 760 K, a single-staged flame transforms into a two-staged one, and it returns to the single-staged structure with further increment in inlet temperature (e.g. $T_{in} = 1100$ K), manifesting the counterpart of NTC behavior in flame propagation. For the two-staged flame structure, the first stage represents cool flame and second one corresponds to hot flame; and the higher the inlet temperature, the closer the cool flame to the inlet.

Further, the flame speed corresponding to different inlet temperatures at three computation domain lengths is presented in Fig. 3(a), which shows the non-monotonic change in laminar flame speed with the upstream affected by LTC reactivity. Taking the computation domain of $L = 2$ cm for example, the flame speed at $T_{in} = 700$ K is approximate $S_u = 1.1$ m/s while it increases up to $S_u = 20$ m/s at $T_{in} = 860$ K where two-staged flame structure emerges. As the inlet temperature further increases to $T_{in} = 960$ K, the flame speed shows a decreasing trend due to the weakend LTC reactivity in NTC regime, and it then increases again with further increment in inlet temperature at high-temperature region.

It should be noted that both temperature increment and partial reaction should affect the flame speed in NTC and higher

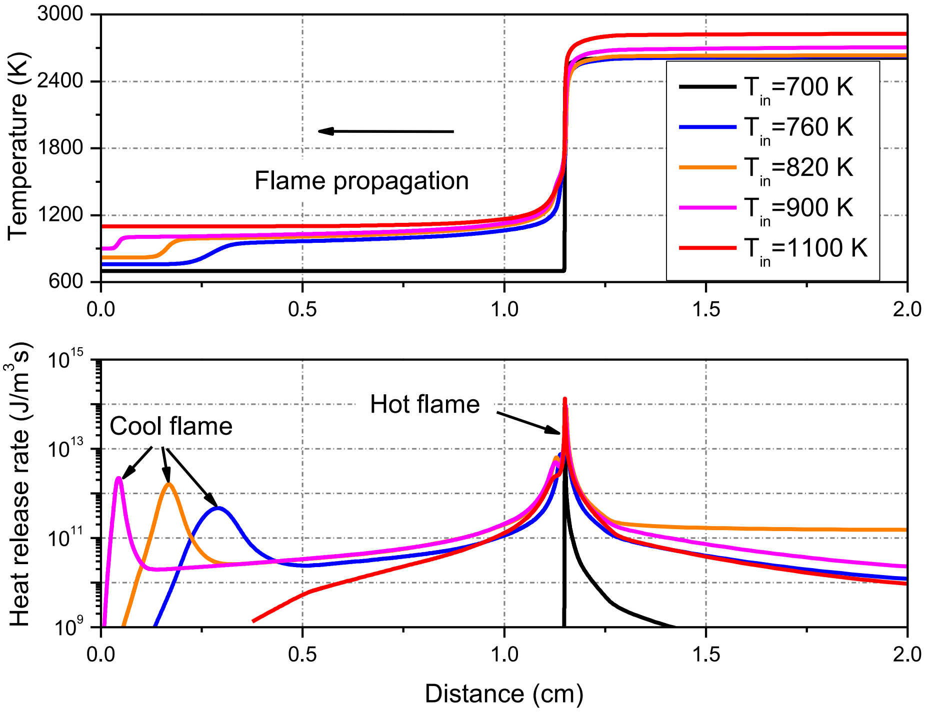

Fig. 2. Profile of temperature and heat release rate of premixed steady flame propagation for stoichiometric n-heptane/air mixture at pressure $P_0 = 40$ atm.

temperature regimes, and their effects are largely coupled. To further evaluate their individual contribution and isolate the role of the LTC in flame propagation with elevated inlet temperatures, simulations based on Jetsurf 1.0 are performed and compared with those obtained using the current mechanism in variable domain length, as shown in Fig. 3(b). It presents that for low inlet temperature ($T_{in} < 700$ K), the flame speed obtained from both mechanisms increases slowly with the inlet temperature and seems insensitive to domain length, implying negligible role of auto-ignition in flame propagation, although quantitative difference does exist in flame speed between these two mechanisms. For high enough inlet temperature (e.g. $T_{in} = 1100$ and 1200 K), both mechanisms show similar increasing trend in flame speed with very close values, which further implies the negligible influence from the LTC under high enough temperature. For the intermediate temperature regime within NTC, two mechanisms show different trends in flame speed with inlet temperature as well as different dependence on domain length. With LTC, flame speed firstly increases and then decreases with temperature, showing the similar NTC behavior as ignition delay. This implies the inherent non-monotonicity induced by LTC in flame propagation within NTC regime. Therefore, comparing the results of the two mechanisms, it is highly suggested that the source of the variations in the flame speed within NTC regime is mainly due to the reactive intermediates from auto-ignition chemistry.

Meanwhile, it is observed that different from the behavior under normal conditions, the flame speed with partially reactive upstream boundary quantitatively depends on the length of computational domain. It is normally considered that the flame burning flux is an eigen-value of the energy or species conservation equation, which could be uniquely identified by imposing proper boundary conditions. Note that in such cases, the so-called “cold boundary difficulty” is avoided by setting zero reaction rate at upstream boundary for the temperature below a certain value, so that no reaction occurs in the preheat zone. In current cases, the “cold boundary difficulty” is inevitable due to the much higher elevated temperature and more pronounced partial reactions from auto-ignition, so that the basic assumption for the above relations fails and the flame burning flux cannot be uniquely determined any more, as demonstrated by computations in Fig. 3(b) with variable domain lengths. This dependence basically implies the unsteady nature of the auto-ignitive upstream boundary and the critical role of residence time for the auto-ignition-affected flame propagation, similar to the recently identified laminar premixed cool flame [20]. The non-monotonic NTC behavior of the laminar flame propagation nevertheless holds qualitatively for different domain lengths in NTC regime.

To further identify the controlling chemistry in flame propagation, sensitivity analysis of laminar flame speed is investigated at three different initial temperatures, $T_{in} = 600$ K below NTC, $T_{in} = 900$ K within NTC and $T_{in} = 1100$ K beyond NTC regime, as shown in Fig. 4. It is observed that for the case of $T_{in} = 600$ K, the most important reactions are the chain branching reaction $H+O_2=OH+O$ and chain propagation reaction $CO+OH=CO_2+H$, consistent to existing understandings of flame chemistry under normal thermodynamic conditions [42]. For the case of T_{in}=1100 K, the dominant chain branching reaction transforms into $H_2O_2+M=OH+OH+M$, implying the controlling role of auto-ignition chemistry. Unlike the cases of $T_{in} = 600$ K and 1100 K, the dominant chemical reactions of $T_{in} = 900$ K within NTC regime involve typical low-temperature chemistry pathways such as the isomerization reaction $C_7H_{15}O_2=C_7H_{14}OOH$, and the low-temperature chain branching $C_7H_{14}OOHO_2=NC_7KET+OH$. From the above analysis, it is suggested that the involvement of auto-ignition chemistry and the corresponding variation of flame structure should be accounted for in order to understand and describe the flame propagation under elevated thermodynamic conditions, such as those in internal combustion engines [43].

In order to mimic the complex combustion under engine-relevant conditions, the solutions of premixed steady flame are exactly extracted, including local thermodynamic state and species concentration by a point-to-point manner, and then are utilized as the initial condition of the unsteady reactive flow [44–46] in a 1D, planar, constant-volume combustion chamber with reflective and

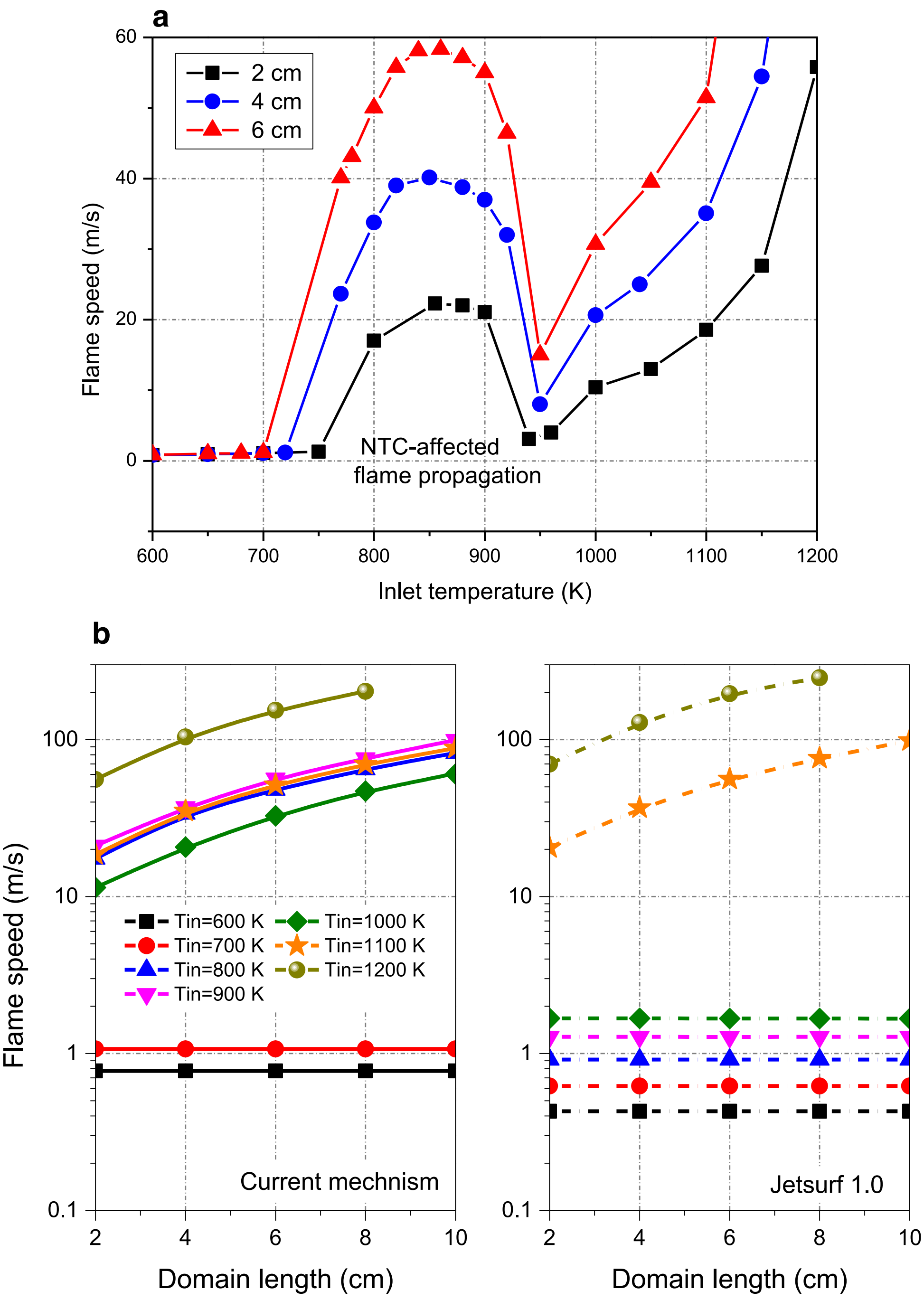

Fig. 3. (a) NTC-affected flame speed as a function of inlet temperature with domain size of 2, 4 and 6 cm. (b) Flame speed variation with domain length at different inlet temperatures using Jetsurf 1.0 and current mechanism for stoichiometric n-heptane/air mixture at $P_0 = 40$ atm.

adiabatic right boundaries. Symmetric condition has been set up at the left boundary and the computation domain length is 4.0 cm. Initially, all hot flame fronts are located at $x = 1.0$ cm in the unsteady reactive flow with a stationary initial state, and then these flame fronts start to propagate, as shown in Fig. 5. The initial flow is static and the initial pressure of $P_0 = 40$ atm is uniformly distributed in the computational domain. Due to the thermal and kinetic inhomogeneities caused by pressure wave disturbances, local auto-ignition may occur at its most favorable locations across the combustion chamber, such as in the end-gas region [46] or even in the preheat zone of a propagating flame [47]. The subsequent evolutions of main flame propagation, auto-ignition (AI) initiation and AI reaction front propagation are then investigated in details.

3.2. Auto-ignition scenarios during flame propagation

Figure 6 shows the evolutions of temperature, pressure, heat release rate and species mass fraction for the case with $T_i = 760$ K, below the lower boundary of NTC regime. It is observed that a two-staged flame initially propagates into stationary reactive mixture, with hot flame front located at $x = 1.0$ cm and cool flame front at $x = 1.8$ cm. During the following process, the temperature and pressure of the bulk mixture gradually increase. It is observed that at the reaction front defined by local maximum temperature gradient, the peaks of heat release rate for hot and cool flame are approximately $Q_{max} = 10^{13}$ and 10^{11} J/m^{3}s, respectively, indicating two-orders of magnitude higher heat release rate from the hot

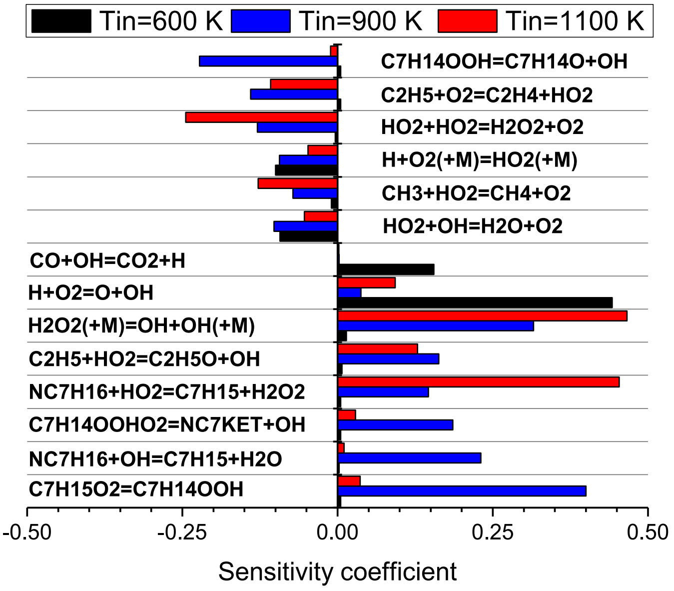

Fig. 4. Sensitivity analysis of laminar flame speed for stoichiometric n-heptane/air mixture at $T_{in} = 600–1000$ K and $P_0 = 40$ atm.

flame. While at other locations, both temperature and pressure fields are largely uniform, without obvious disturbance by acoustic waves. Until $t = 248$ μs, end-gas mixture experiences the first-stage auto-ignition and its temperature rises simultaneously, such that the cool flame front disappears at $x = 2.35$ cm. Therefore, a portion of n-C_7H_{16} (approximate 63.4%) is oxidized by low-temperature combustion and CH_2O concentration increases to the maximum level in the bulk mixture, implying chemical reactivity of the cool flame. Subsequently, an auto-ignition event occurs around the location where cool flame disappears around $x = 2.4$ cm, and two AI flame fronts develop and spread out accompanied with strong pressure waves. The AI flame spreading to the left interacts with the hot flame, burns up the mixture trapped in the middle and eventually leads to a local pressure mutation of $P_{max} = 30$ atm, while the one spreading to the right develops into a detonation wave, with a very high pressure peak of $P_{max} = 600$ atm and heat release rate peak of $Q_{max} = 10^{15}$ J/m^{3}s, two-orders of magnitude higher than the regular hot flame.

The transient propagation speeds of all reaction fronts involved are shown in Fig. 7, with the local sound speed plotted as a reference. It is observed that the hot flame and cool flame initially propagate with a mean deflagration speed of $\nu = 40$ and 28 m/s, respectively, with a weak oscillating behavior due to acoustic wave disturbances in current constant-volume combustion chamber. Subsequently, an auto-ignition event is initiated at $x \approx 2.3$ cm and produces two fast-propagating reaction fronts 1 and 2. The AI front 1 develops from subsonic mode into supersonic mode while the AI flame front 2 quickly develops into supersonic mode with the maximum speed of $\nu_{max} = 2460$ m/s which then gradually decreases to $\nu = 2150$ m/s. This speed is much higher than the CJ detonation speed of $\nu_{CJ} = 1854$ m/s for stoichiometric n-heptane/air mixture at $T_i = 1200$ K and $P_0 = 70$ atm.

Figure 8 shows the evolutions of temperature, pressure, heat release rate and typical species mass fraction for $T_i = 820$ K, close to the NTC lower boundary. It is observed that in contrast to the case of $T_i = 760$ K, auto-ignition not only occurs at the location where cool flame front disappears, but also at end-wall region, resulting in more complex combustion mode with multiple flame fronts. When $t = 174$ μs, auto-ignition is initiated at $x = 2.5$ cm and generates two fast-propagating AI flame fronts. Similar to the previous case, the one spreading to the right develops into a detonation wave with $P_{max} = 800$ atm and $Q_{max} = 10^{16}$ J/m^{3}s. However, another AI front originated from end-wall region quickly propagates to the left of combustion chamber, with $P_{max} = 600$ atm and $Q_{max} = 10^{15}$ J/m^{3}s. Eventually, the two AI flame fronts collide at $x = 3.4$ cm, resulting in a substantial local pressure mutation with $P_{max} > 1800$ atm. Meanwhile, it is observed that there are new AI spots induced by pressure wave occurring just ahead of AI flame front, which may contribute to the detonation formation. The spatial distributions of OH, CH_2O and n-C_7H_{16} mass fraction are consistent with the evolutions of flame propagation, auto-ignition occurrence and its development in the reactive flow.

Figure 9 shows the evolutions of temperature, pressure, heat release rate and species mass fraction for $T_i = 900$ K, right in the NTC regime under the pressure of 40 atm. Compared with previous two cases, new observations can be obtained as the following. Firstly, there is no apparent auto-ignition event taking place

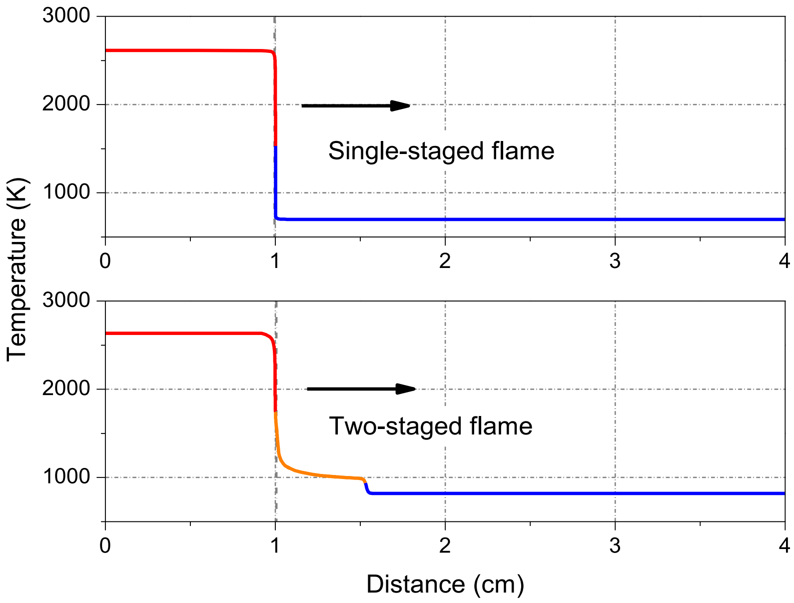

Fig. 5. Initial profiles of single-staged and two-staged flame in the unsteady reaction flow with left symmetric boundary and right wall boundary.

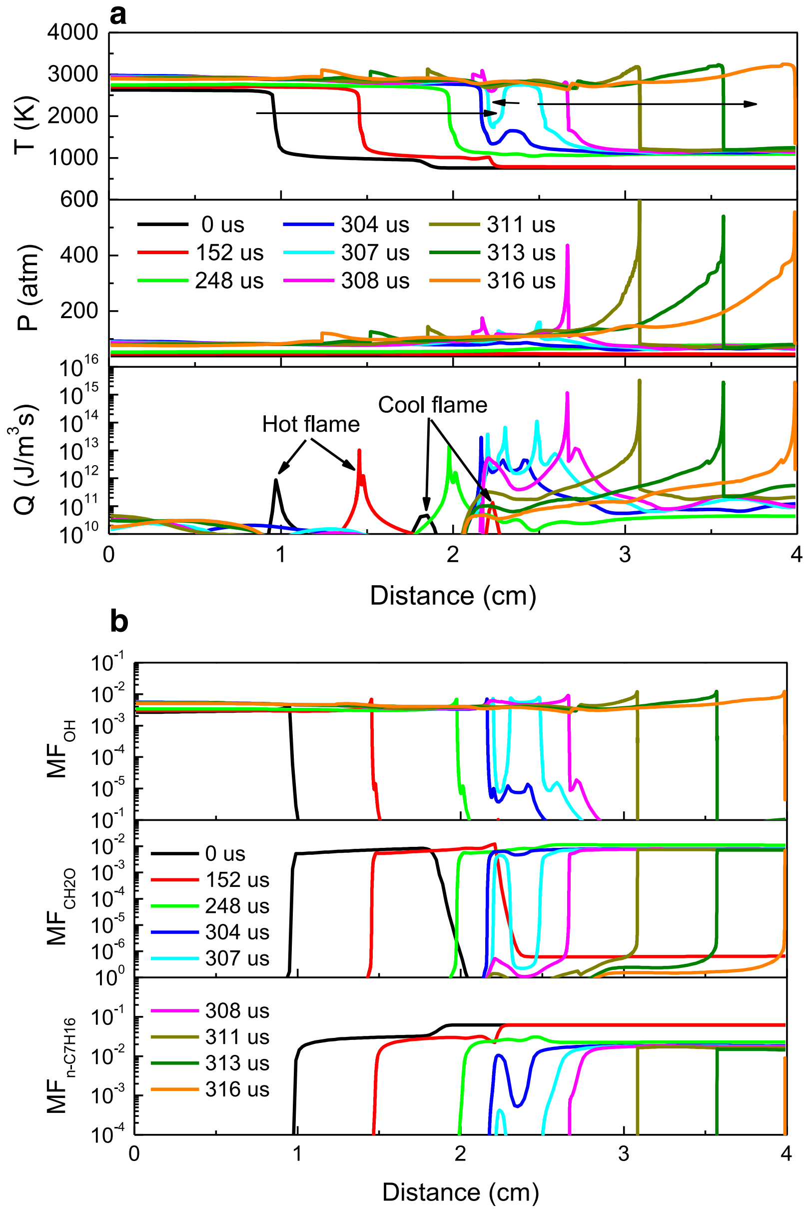

Fig. 6. Evolutions of (a) temperature T (K), pressure P (atm), heat release rate Q (J/m^{3}s) and (b) mass fraction of OH, CH_2O and n-C_7H_{16} species for T_i = 760 K and $P_0 = 40$ atm.

at the location ahead of hot flame front. This is due to the fact that the corresponding cool flame temperature rise is much lower, which leads to reduced upstream cool flame reactivity. Secondly, for the end-wall auto-ignition, it does not immediately develop into a detonation wave but firstly experiences a supersonic combustion process without strong discontinuity in local pressure field. The reason for this is that some mixture in the upstream of AI flame front reaches the auto-ignition threshold and tends to experience auto-ignition simultaneously, as shall be analyzed later. Thirdly, during the evolution of the AI front in the end-gas region, the variations in pressure peak from $P_{max} = 200$ atm at $t = 155$ s to $P_{max} = 570$ atm at $t = 158$ s as well as substantial changes in heat release rate suggest that there is a transition in combustion mode, and this can also be identified by the characteristic spontaneous ignition front propagation speed presented in the following section.

With initial temperature further increased to T_i = 1100 K beyond NTC regime, there is only hot flame propagation, as shown in Fig. 10. It is observed that an auto-ignition is initiated at t = 288.58 s and subsequently generates an AI flame front with a much flatter temperature gradient. Unlike cases of T_i = 760 and 820 K, the pressure amplitude for current AI flame is $P_{max} = 170$ atm before interacting with the hot flame, without observable shock wave due to the much faster flame propagation. Meanwhile, the heat release rate peak with $Q_{max} = 10^{14}$ J/m^{3}s for the AI flame is close to that of the initial hot flame, and one-order of magnitude lower than that of the normal detonation wave as shown in Fig. 6. These observations indicate that end-wall auto-ignition does not develop into a detonation wave and appears to fall into a conventional engine knock. Actually, it is shown in the following that the AI reaction front at $T_i = 1100$ K propagates at the level of spontaneous ignition front propagation speed, in which subsequent auto-ignition occurs due to the substantial chemical reactivity gradient ahead of AI flame front. This can be also supported by the gradual increases of OH mass fraction and decreases of CH_2O and n-C_7H_{16} mass fraction in the unburned zone.

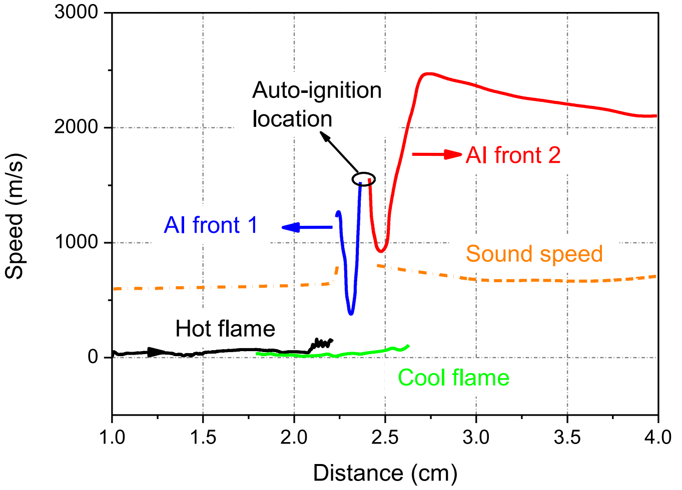

Fig. 7. Transient flame speed and sound speed ahead of different flame fronts for $T_i = 760$ K.

Figure 11 shows the transient propagation speed of different reaction fronts with the local speed of sound as a reference. It is observed that the transient AI front propagation speed of $T_i = 1100$ K case is much higher than that of $T_i = 900$ K. Meanwhile, both auto-ignition events issue supersonic propagating flame front; however, it fails to develop into a detonation wave for the AI flame of $T_i = 1100$ K case in terms of flame thickness, peak heat release rate and peak pressure. Further, the comparison of hot flame speed between $T_i = 900$ and 1100 K case shows that due to the absence of cool flame, the mean propagation speed for $T_i = 1100$ K case is lower even though its initial temperature is much higher, as shown in Fig. 12(a), consistent with the results of the NTC-affected laminar flame speed shown in Fig 3. Figure 12(b) further gives the distributions of temperature and mass fraction of typical species for OH, H and CH_2O during the flame propagation at $T_i = 900$ and 1100 K. It is observed that although the temperature is much lower, the mass fraction of typical species (OH, H and CH_2O) ahead of flame front for $T_i = 900$ K case are always higher, especially for the CH_2O mass fraction. Above observations basically suggest the sig-

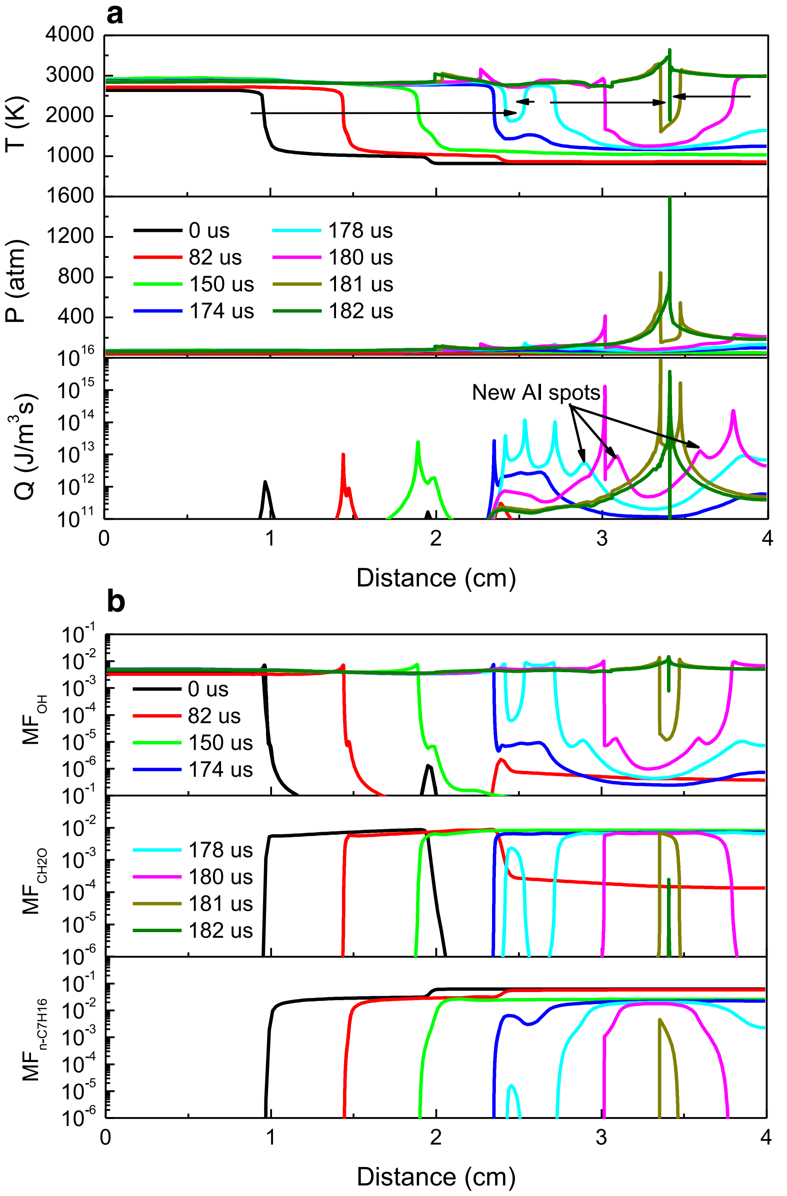

Fig. 8. Evolutions of (a) temperature T (K), pressure P (atm), heat release rate Q (J/m^{3}s) and (b) mass fraction of OH, CH_2O and n-C_7H_{16} species for $T_i = 820$ K.

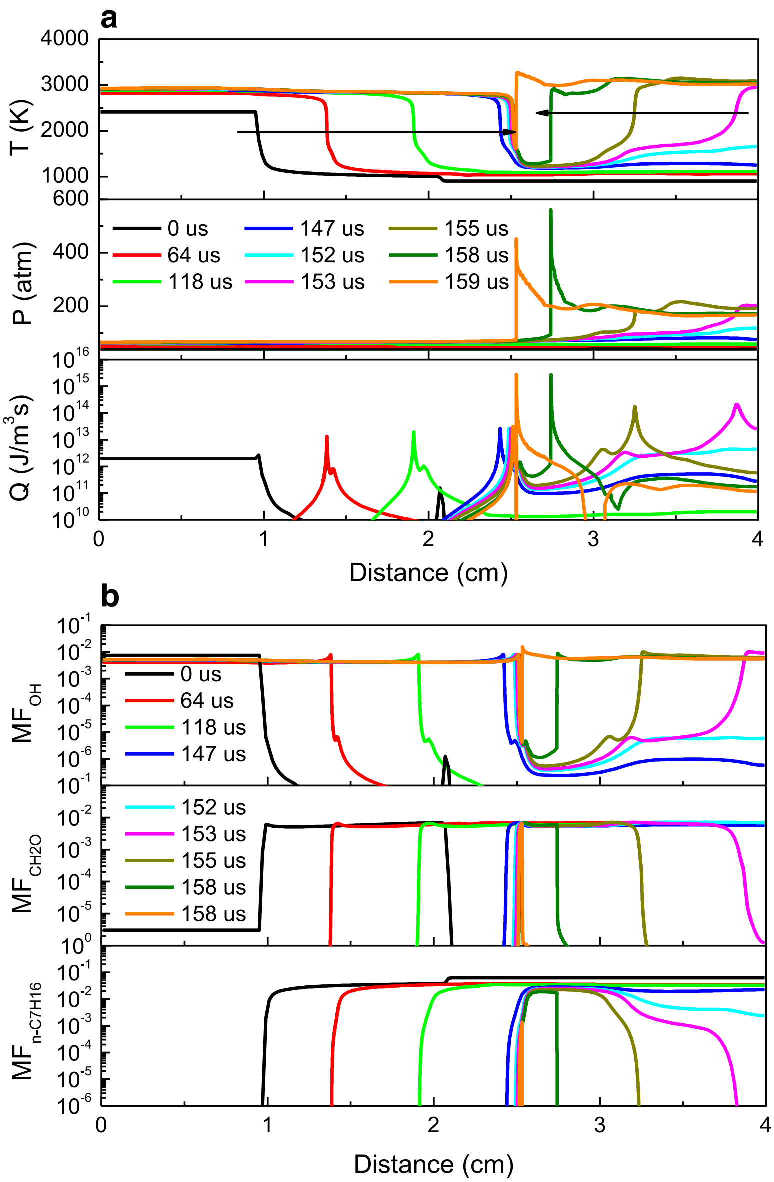

Fig. 9. Evolutions of (a) temperature T (K), pressure P (atm), heat release rate Q (J/m^{3}s) and (b) mass fraction of OH, CH_2O and n-C_7H_{16} species for $T_i = 900$ K.

nificant role of NTC chemistry on the propagation of a flame front in the unsteady reactive flow, potentially by elevated thermodynamic conditions and the feed of active intermediates from low-temperature chemistry.

From the comparison and analysis from Figs. 11 to 12, it is then evident that NTC could significantly promote flame propagation, and the sensitivity of ignition delay to temperature within the NTC regime largely affects the combustion mode of the AI front. Another interesting point could be raised among these cases is about the location that auto-ignition could occur. This could be analyzed by investigating the detailed local temperature and pressure history on a case-by-case basis, since in general, a location achieving auto-ignition or not primarily depends on its pressure and temperature trajectory. In any of these complicated scenarios, both pressure fluctuation and local heat release from slow oxidation contribute to the pressure and temperature history and leads to the eventual observations.

In order to clarify the combustion mode during local auto-ignition development, the spontaneous propagation speed introduced by Zel'dovich [8] is further discussed here:

$$S_{ig} = \left(\left| \frac{d\tau}{dT} \right| \cdot |\nabla T| \right)^{-1} \tag{1}$$

where S_{ig} is the spontaneous ignition front propagation speed and τ the ignition delay time for the homogeneous mixture at the average or bulk temperature and pressure. S_{ig} addresses that combustion wave propagates forward as a result of spontaneous ignition of local mixture. If S_{ig} is close to or comparable to the speed of sound, the combustion wave can be coupled to the acoustic wave, eventually leading to a detonation wave. When S_{ig} approaches infinity, thermal explosion is the corresponding physical phenomenon where all the homogeneous mixture auto-ignites simultaneously [8,9,48].

The profiles of temperature and spontaneous ignition front propagation speed for $T_i = 900$ and 1100 K are further plotted in Fig. 13, corresponding to the instant of 10% maximum heat release rate of end-wall auto-ignition. It is observed that the temperature field is relatively uniform for $T_i = 1100$ K case, and consequently the spontaneous ignition front propagation speed is significantly higher, with a mean $S_{ig} > 10{,}000$ m/s. This propagation speed is

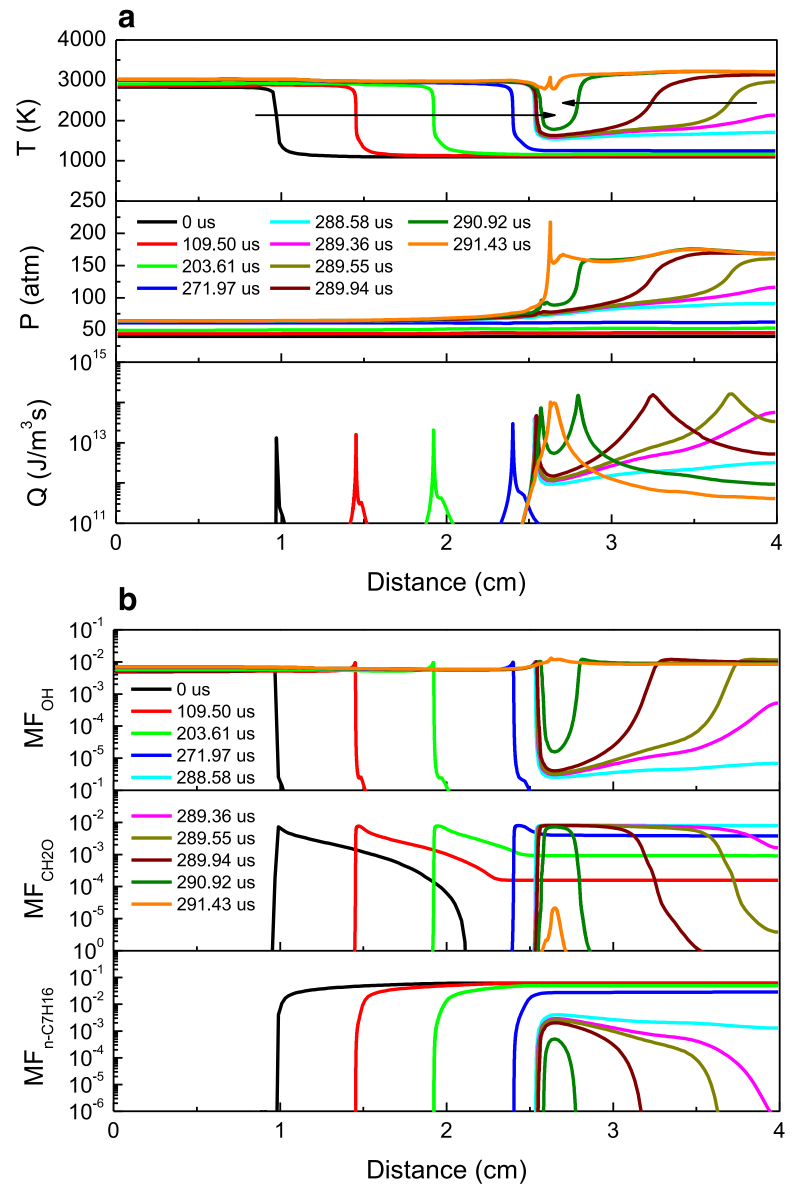

Fig. 10. Evolutions of (a) temperature T (K), pressure P (atm), heat release rate Q (J/m^{3}s) and (b) mass fraction of OH, CH_2O and n-C_7H_{16} species for T_i = 1100 K.

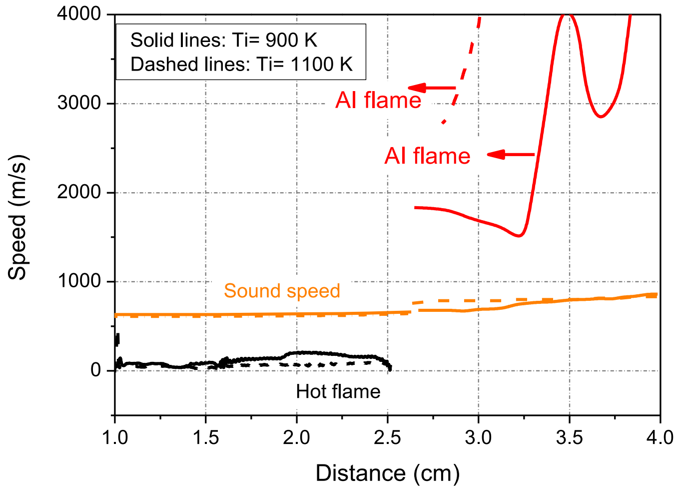

Fig. 11. Transient flame speed and sound speed ahead of different flame fronts for $T_i = 900$ and 1100 K.

much higher than that of local sound with $a \approx$ 680 m/s, leading to negligible interactions between the reaction front and pressure wave, such that the combustion mode is dominant by the spontaneous ignition. For the case of $T_i = 900$ K, the spontaneous ignition front speed S_{ig} is much lower across the domain and ranges from supersonic to subsonic modes. This then leads to more significant effects of pressure wave on the development of reaction fronts, and facilitates the formation of detonation wave. Therefore, the AI reaction front induced by end-wall auto-ignition propagates with spontaneous propagation mode for $T_i = 1100$ K, while there is a mode transition to detonation for the case of $T_i = 900$ K, consistent with the simulation results shown in Figs. 8–10.

3.3. Prediction of auto-ignition timing

Now we have demonstrated the evolutions of flame propagation, auto-ignition and pressure/shock waves with different initial temperatures. To further analyze the auto-ignition process, instantaneous thermodynamic state of auto-ignition location is extracted and then utilized to calculate the instantaneous ignition

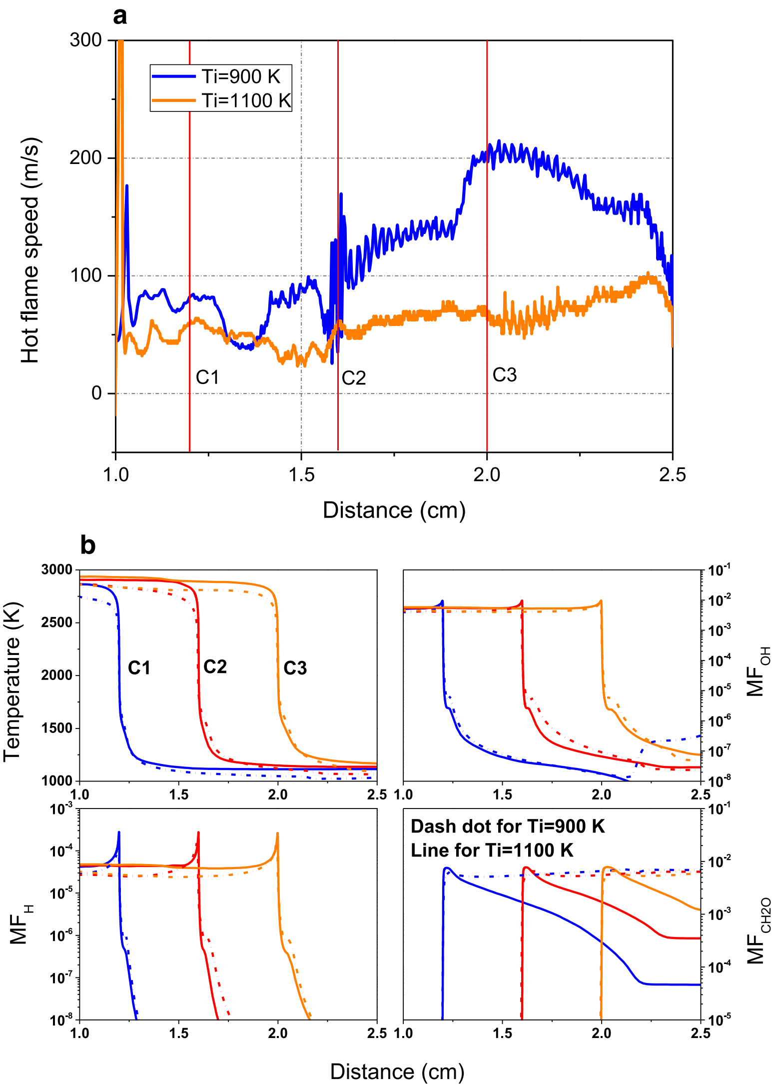

Fig. 12. (a) Comparison of hot flame speed between $T_i = 900$ and 1100 K case. (b) Temperature and species mass fraction of three different scenarios during flame propagation.

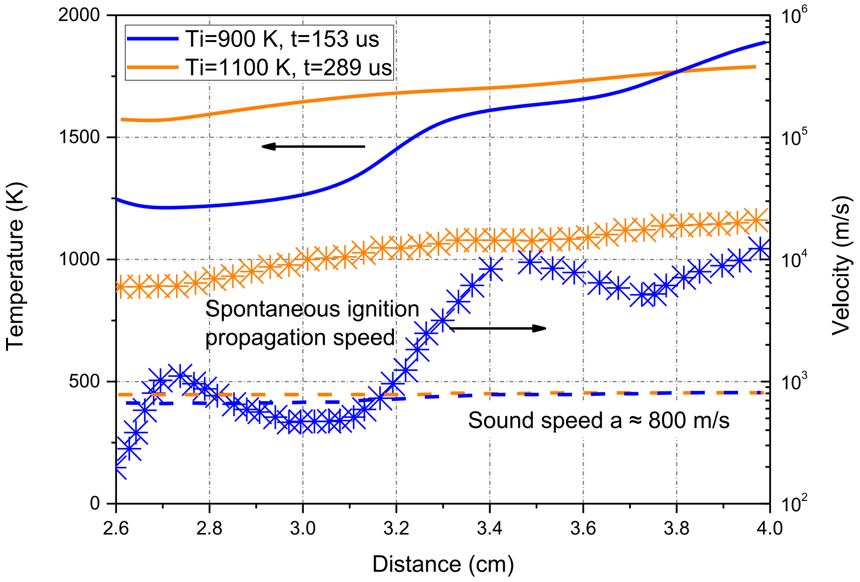

Fig. 13. Comparison of temperature and AI front speed between $T_i = 900$ and 1100 K case.

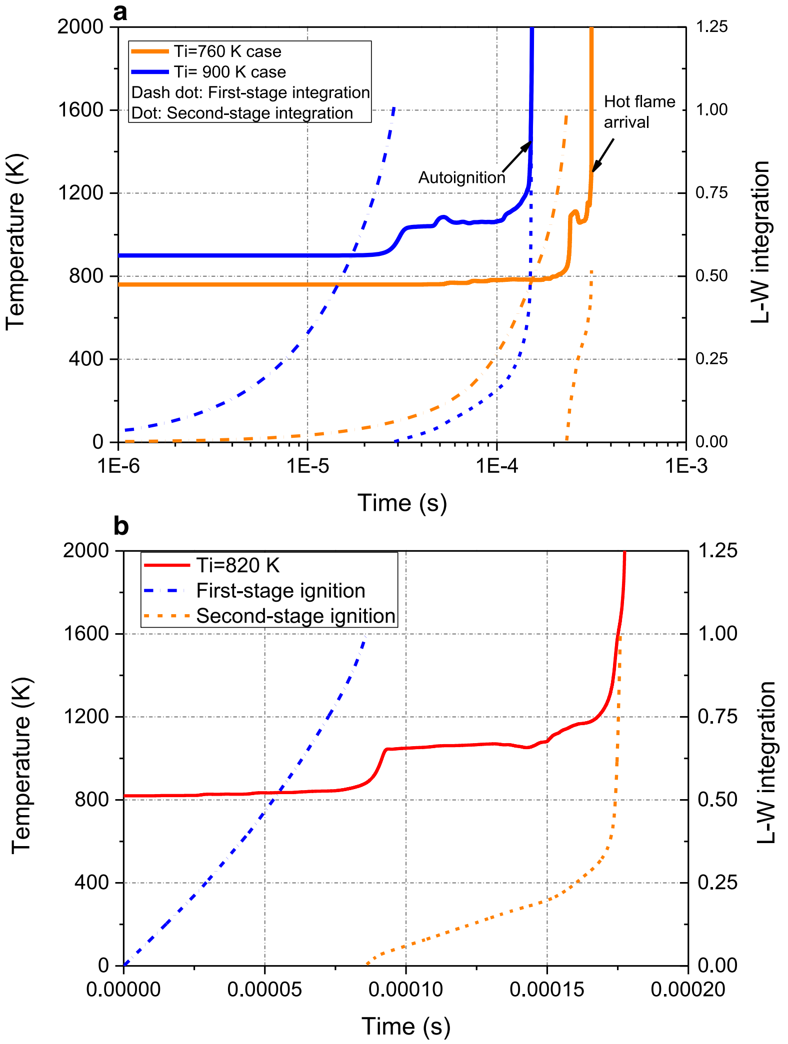

Fig. 14. Temperature evolution of (a) end-wall auto-ignition at $T_i = 760$ and 900 K and (b) auto-ignition ahead of flame front at $T_i = 820$ K and corresponding staged Livengood–Wu integration.

delay based on current n-heptane mechanism. Subsequently, a recently developed two-staged Livengood–Wu (L–W) integration method [49] is introduced with the capacity of accommodating the LTC and change of thermodynamic conditions at cool flame state. The formula of two-staged L–W integral used for low- and high-temperature auto-ignition prediction can be expressed as:

$$1 = \int_{t_0}^{t_1} \frac{dt}{\tau_1(T,\ P)} \tag{2}$$

$$1 = \int_{t_1}^{t_2} \frac{dt}{\tau'(T',\ P')} \tag{3}$$

where t_0 is the initial time when chemistry becomes important, t_1 the time for the appearance of cool flame, t_2 the instant for the major ignition, and τ_1 and τ' corresponds to the first-stage ignition delay and second-stage ignition delay (τ_2 in NTC regime or τ_h in higher temperature regime), respectively. Previous work [49] has validated its enhanced performance in the prediction of two-stage auto-ignition timing under extensive HCCI engine conditions.

As stated in L–W equation, the integration is proposed to predict the auto-ignition timing under variable thermodynamic conditions by using the inverse of ignition delay at constant volume conditions as an indicator for chemical reactivity. If the integral attains a value of unity before end-gas has been entirely consumed by flame front, auto-ignition will occur. Otherwise, the end-gas will be burned up by the propagating main flame. Figure 14 shows the results of temperature evolution and corresponding staged L–W integration for different auto-ignition events. For the end-wall auto-ignition events at $T_i = 760$ and 900 K, the first-stage auto-ignition of both cases are well predicted by the first-stage L–W integral. For the second-stage auto-ignition, the integral value for $T_i = 760$ K just attains a level of approximately 0.5 when the hot flame arrives, demonstrating that the local mixture is consumed by the propagating hot flame rather than auto-ignition; while for $T_i = 900$ K case, the second-stage integral gradually increase to unity before the hot flame arrival, demonstrating the continuously accumulated reaction progress due to auto-ignition. To explain the auto-ignition event ahead of hot flame front, the data from the location of $x = 2.6$ cm has been processed for the cases of $T_i = 820$ K, as shown in Fig. 14(b). It is seen that both integrals well predict the first- and second-stage auto-ignition timing, with the integral value continuously increasing to unity. This analysis further indicates the significant role of the LTC in auto-ignition phenomena, which not only modifies the thermodynamic state, but also enhances the local chemical reactivity.

3.4. Combustion mode and knocking intensity

It is suggested that the pressure peak and knocking intensity greatly depend on combustion mode during local auto-ignition

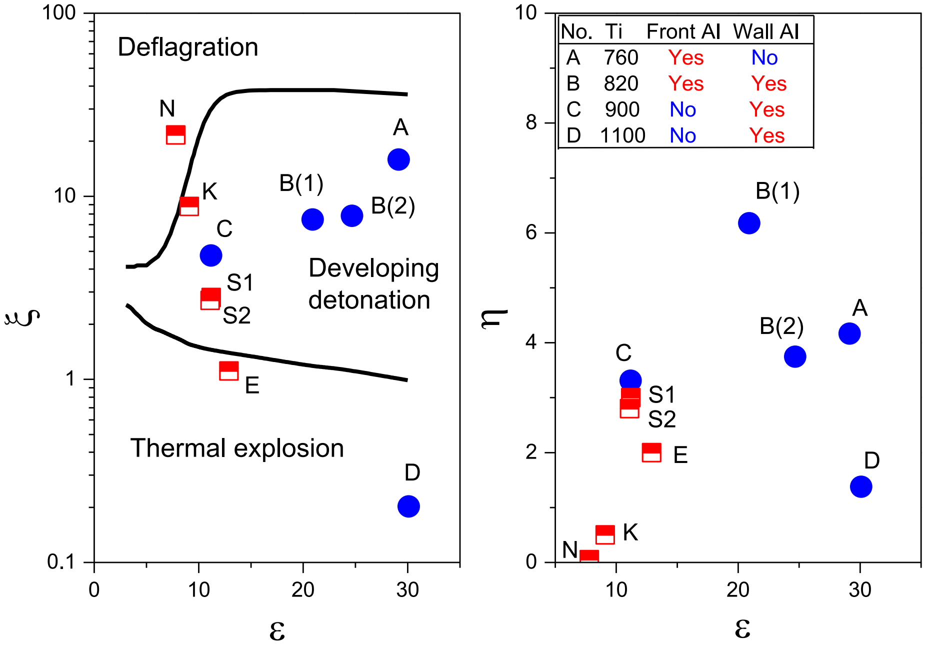

Fig. 15. Summary of combustion mode and knocking intensity in non-dimensional diagrams of (ξ, ε) and (η, ε). The read block symbols respectively present normal combustion (N), knock(K), super-knock (S) and thermal explosion (E) from Kalghatgi and Bradley's work [14].

development [15,46]: auto-ignition can induce high amplitude of pressure wave similar to conventional knock while (developing) detonation wave can cause extremely high amplitude of shock wave as observed in super-knock. To address this relation, further analysis is performed based on the 1D diagrams. According to the "detonation peninsula" theory proposed by Bradley et al. [9–10], a non-dimensional parameter, ξ, describing the coupling between acoustic wave and reaction front propagation, can be defined as:

$$\xi = a/u_a = (\partial T/\partial r)(\partial \tau_i/\partial T)a \tag{4}$$

where a is local sound speed, u_a AI flame speed and r the spatial coordinate of reactive zone.

And meanwhile, a second non-dimensional parameter, ε, assessing the rapidity of reaction energy release, is expressed by:

$$\varepsilon = (r_0/a)/\tau_e \tag{5}$$

where r_0 represents the initial radius of hot spot determined by temperature gradient, and τ_e is the excitation time defined as the time interval between 5% and maximum heat release rate.

In order to fully characterize the knocking intensity, an additional non-dimensional parameter is introduced here:

$$\eta = (P_{max} - P_{AI})\ /(P_{isoc} - P_{AI}) \tag{6}$$

where P_{AI} is the pressure at auto-ignition timing (corresponding to the instant of 10% maximum heat release rate in current work), P_{max} the maximum pressure during AI flame propagation, and P_{isoc} the maximum pressure obtained from theoretical isochoric combustion based on the initial auto-ignition conditions.

Based on the above definitions, the non-dimensional parameters ξ and ε are evaluated at the main auto-ignition timing corresponding to the instant of 10% maximum heat release rate to accommodate the cool flame heat release, while non-dimensional parameter η is evaluated during auto-ignition development. Finally, two non-dimensional diagrams, (ξ, ε) and (η, ε), are plotted, to evaluate and analyze the combustion mode and knocking intensity for $T_i = 760$–1100 K cases, as summarized in Fig. 15, where B(1) represents the auto-ignition ahead of flame front (i.e. front AI) and B(2) the end-wall auto-ignition (i.e. wall AI) for the 820 K case. Previous experimental work by Kalghatgi and Bradley [14] showed that as engine combustion process shifts from normal combustion to knocking combustion and thermal explosion, ξ quickly decreases and ε increases. For current work, it is observed that as initial temperature increases, there is a transition for the auto-ignition position from the location ahead of flame front to end-wall region, accompanied by obvious variations in combustion mode and knocking intensity. The diagram (ξ, ε) shows that the combustion mode for $T_i = 760$–900 K cases is located in developing detonation regime, while the one for $T_i = 1100$ K case is in thermal explosion regime with a higher propagation speed but much lower pressure magnitude. These observations demonstrate that with NTC chemistry, (developing) detonation wave with high pressure peak could be triggered even at much lower temperatures and at different locations of the combustion field. More importantly, the diagram (η, ε) shows that most developing detonation cases (point A, B(2) and C) correspond to a knocking intensity of approximate $\eta = 4$, however, it attains an level of $\eta = 6.2$ for B(1) case, demonstrating the significant effect of the LTC on knocking intensity. While for the scenario with a much higher initial temperature $T_i = 1100$ K (point D), the knocking intensity caused by thermal explosion is much less severe. Therefore, the combination of these non-dimensional diagrams well characterizes different combustion modes and knocking intensity, with more complete guidance on knocking combustion.

4. Conclusions

In the present study, one-dimensional simulations are performed to study the auto-ignition and flame propagation of n-heptane/air mixture in a broad temperature range including NTC regime under elevated pressure conditions. Fundamental insights for low-temperature chemistry effect on knocking combustion are provided. It shows that affected by NTC chemistry, steady premixed flame propagation shows a two-stage behavior, including both hot and cool flame segments. With the increases of inlet temperature, the flame speed shows the corresponding non-monotonic NTC behavior: it first increases with increasing initial temperature, then decreases with further increasing initial temperature in NTC regime, and increases again with the initial temperature beyond

NTC regime. Further calculations show such behavior qualitatively retains with variable domain length, while the quantitative dependences of flame speed and structure on domain length with elevated temperature basically implies that flame speed is not an eigenvalue anymore due to the aggravated cold boundary difficulty with auto-ignition inlet temperatures.

These steady premixed flames are then utilized as the initial conditions of the unsteady simulations in a one-dimensional, planar, constant-volume combustion chamber with adiabatic and reflective boundary. The results show that different auto-ignition scenarios are identified during two-staged and single-staged flame propagation. As initial temperature increases, there is a transition for auto-ignition position from the location ahead of flame front to end-wall region. The transition of auto-ignition position is accompanied by obvious variations in flame speed, local pressure and heat release rate, suggesting that these auto-ignition events induce different auto-ignitive reaction fronts with various combustion modes and pressure peaks. Chemical structure analysis further demonstrates the essential role of reactive intermediates feeding within the NTC regime, which consequently leads to faster flame propagation.

To predict auto-ignition timing in these scenarios, a recently developed staged Livengood-Wu correlation has been utilized to analyze the auto-ignition processes occurring both at end-wall region and ahead of flame front. The results show that both first- and second-stage Livengood–Wu integral gradually increase to unity at the simulated low- and high-temperature auto-ignition events, respectively. Such prediction further identifies the controlling role of low temperature chemistry in modifying the thermodynamic state and local chemical reactivity, triggering auto-ignition at different favored locations.

Finally, two non-dimensional diagrams are introduced to analyze the combustion mode and knocking intensity. It is found that with low temperature chemistry, the combustion mode with (developing) detonation could be induced at much lower initial temperatures, while thermal explosion is triggered at even higher initial temperature with a lower pressure peak, leading to conventional engine knock. Moreover, depending on the subsequent evolutions of different reaction fronts, knocking intensity could vary even with the same combustion mode determined by initial hot-spots properties. The most severe knock is actually induced in the case with initial temperature right below the NTC regime and involves the collision of different reaction fronts from multiple hot-spots.

Acknowledgment

This work was supported by National Natural Science Foundation of China (Grant No. 51476114), China Postdoctoral Science Foundation (2016M590201) and 2016 Industry, Education and Research Foundation of Tianjin University. PZ is supported by the startup funding at Oakland University.

References

[1] N. Fraser, H. Blaxill, G. Lumsden, M. Bassett, Challenges for increased efficiency through gasoline engine downsizing, SAE Int. J. Engines 2 (2009) 991–1008.

[2] J.Y. Pan, G.Q. Shu, H.Q. Wei, Interaction of flame propagation and pressure waves during knocking combustion in spark-ignition engines, Combust. Sci. Technol. 186 (2014) 192–209.

[3] N. Peters, B. Kerschgens, G. Paczko, Super-knock prediction using a refined theory of turbulence, SAE Int. J. Engines 6 (2013) 953–967.

[4] C. Dahnz, U. Spicher, Irregular combustion in supercharged spark ignition engines pre-ignition and other phenomena, Int. J. Engine Res. 11 (2011) 485–498.

[5] H. Terashima, M. Koshi, Mechanisms of strong pressure wave generation in end-gas auto-ignition during knocking combustion, Combust. Flame 162 (2015) 1944–1956.

[6] Z. Wang, Y. Qi, X. He, J. Wang, S. Shuai, C.K. Law, Analysis of pre-ignition to super-knock: hotspot-induced deflagration to detonation, Fuel 144 (2015) 222–227.

[7] N. Kawahara, E. Tomita, Y. Sakata, Auto-ignited kernels during knocking combustion in a spark-ignition engine, Proc. Combust. Inst. 31 (2007) 2999–3006.

[8] Y.B. Zeldovich, Regime classification of an exothermic reaction with nonuniform initial conditions, Combust. Flame 39 (1980) 211–214.

[9] D. Bradley, G.T. Kalghatgi, Influence of auto-ignition delay time characteristics of different fuels on pressure waves and knock in reciprocating engines, Combust. Flame 156 (2009) 2307–2318.

[10] X. Gu, D. Emerson, D. Bradley, Modes of reaction front propagation from hot spots, Combust. Flame 133 (2003) 63–74.

[11] G. Kalghatgi, Developments in internal combustion engines and implications for combustion science and future transport fuels, Proc. Combust. Inst. 35 (2015) 101–115.

[12] D. Bradley, Auto-ignitions and detonations in engines and ducts, Philos, Trans. A Math. Phys. Eng. Sci. 370 (2012) 689–714.

[13] L. Bates, D. Bradley, G. Paczko, N. Peters, Engine hot spots: Modes of auto-ignition and reaction propagation, Combust. Flame 166 (2016) 80–85.

[14] G.T. Kalghatgi, D. Bradley, Pre-ignition and 'super-knock' in turbo-charged spark-ignition engines, Int. J. Engine Res. 13 (2012) 399–414.

[15] J. Rudloff, J.M. Zaccardi, S. Richard, J.M. Anderlohr, Analysis of pre-ignition in highly charged SI engines: emphasis on the auto-ignition mode, Proc. Combust. Inst. 34 (2013) 2959–2967.

[16] K.P. Grogan, S.S. Goldsborough, M. Ihme, Ignition regimes in rapid compression machines, Combust. Flame 162 (2015) 3071–3080.

[17] H.G. Im, P. Pal, M.S. Wooldridge, A.B. Mansfield, A regime diagram for auto-ignition of homogeneous reactant mixtures with turbulent velocity and temperature fluctuations, Combust. Sci. Technol. 187 (2015) 1263–1275.

[18] C.K. Law, P. Zhao, NTC-affected ignition in nonpremixed counterflow, Combust. Flame 159 (2012) 1044–1054.

[19] J.F. Griffiths, J.P. MacNamara, C.G.W. Sheppard, D.A. Turton, B.J. Whitaker, The relationship of knock during controlled auto-ignition to temperature inhomogeneities and fuel reactivity, Fuel 81 (2002) 2219–2225.

[20] P. Zhao, W. Liang, S. Deng, C.K. Law, Initiation and propagation of laminar premixed cool flames, Fuel 166 (2016) 477–487.

[21] S. Deng, P. Zhao, M.E. Mueller, C.K. Law, Auto-ignition-affected stabilization of laminar nonpremixed DME/air coflow flames, Combust. Flame 162 (2015) 3437–3445.

[22] M. Yao, Z. Zheng, H. Liu, Progress and recent trends in homogeneous charge compression ignition (HCCI) engines, Prog. Energ. Combust. 35 (2009) 398–437.

[23] W. Sun, S.H. Won, X. Gou, Y. Ju, Multi-scale modeling of dynamics and ignition to flame transitions of high pressure stratified n-heptane/toluene mixtures, Proc. Combust. Inst. 35 (2015) 1049–1056.

[24] Y. Ju, W. Sun, M.P. Burke, X. Gou, Z. Chen, Multi-timescale modeling of ignition and flame regimes of n-heptane-air mixtures near spark assisted homogeneous charge compression ignition conditions, Proc. Combust. Inst. 33 (2011) 1245–1251.

[25] J.B. Martz, G.A. Lavoie, H.G. Im, R.J. Middleton, A. Babajimopoulos, D.N. Assanis, The propagation of a laminar reaction front during end-gas auto-ignition, Combust. Flame 159 (2012) 2077–2086.

[26] P. Dai, Z. Chen, S. Chen, Y. Ju, Numerical experiments on reaction front propagation in n-heptane/air mixture with temperature gradient, Proc. Combust. Inst. 35 (2015) 3045–3052.

[27] P. Dai, Z. Chen, Supersonic reaction front propagation initiated by a hot spot in n-heptane/air mixture with multistage ignition, Combust. Flame 162 (2015) 4183–4193.

[28] A. Robert, S. Richard, O. Colin, T. Poinsot, LES study of deflagration to detonation mechanisms in a downsized spark ignition engine, Combust. Flame 162 (2015) 2788–2807.

[29] Y. Qi, Z. Wang, J. Wang, X. He, Effects of thermodynamic conditions on the end gas combustion mode associated with engine knock, Combust. Flame 162 (2015) 4119–4128.

[30] G. Lecocq, S. Richard, J.B. Michel, L. Vervisch, A new LES model coupling flame surface density and tabulated kinetics approaches to investigate knock and pre-ignition in piston engines, Proc. Combust. Inst. 33 (2011) 3105–3114.

[31] C.S. Yoo, T.F. Lu, J.H. Chen, C.K. Law, Direct numerical simulations of ignition of a lean n-heptane/air mixture with temperature inhomogeneities at constant volume: parametric study, Combust. Flame 158 (2011) 1727–1741.

[32] M. Mehl, W.J. Pitz, C.K. Westbrook, H.J. Curran, Kinetic modeling of gasoline surrogate components and mixtures under engine conditions, Proc. Combust. Inst. 33 (2011) 193–200.

[33] A. Miyoshi, KUCRS Software Library for update information. The program uses THERM program for thermodata generation. http://www.frad.t.u-tokyo.ac.jp/∼miyoshi/KUCRS/

[34] H.K. Ciezki, G. Adomeit, Shock-tube investigation of self-ignition of n-heptane-air mixtures under engine relevant conditions, Combust. Flame 93 (1993) 421–433.

[35] A.P. Kelley, A.J. Smallbone, D.L. Zhu, C.K. Law, Laminar flame speeds of C5 to C8 n-alkanes at elevated pressures: Experimental determination, fuel similarity, and stretch sensitivity, Proc. Combust. Inst. 33 (2011) 963–970.

[36] B. Sirjean, E. Dames, D.A. Sheen, X.-Q. You, C. Sung, A.T. Holley, F.N. Egolfopoulos, H. Wang, et al., A high-temperature chemical kinetic model of n-alkane oxidation, JetSurF version 1.0, 2009. (http://melchior.usc.edu/JetSurF1.0).

[37] R.J. Kee, J.F. Grcar, M.D. Smooke, J.A. Miller, A program for modeling steady, laminar, one-dimensional premixed flames, Report No. SAND85-8240, Sandia National Laboratories, 1985.

[38] P.N. Brown, G.D. Byrne, A.C. Hindmarsh, VODE: A variable-coefficient ODE solver, SIAM J. Sci. Stat. Comput. 10 (1989) 1038–1051.

[39] Z. Chen, On the extraction of laminar flame speed and Markstein length from outwardly propagating spherical flames, Combust. Flame 158 (2011) 291–300.

[40] W.K. Zhang, Z. Chen, W.J. Kong, Effects of diluents on the ignition of premixed H_2/air mixtures, Combust. Flame 159 (2012) 151–160.

[41] Z. Chen, Studies on the initiation, propagation, and extinction of premixed flames Ph.D. Thesis, Princeton University, Princeton, NJ, USA, 2008.

[42] E. Ranzi, A. Frassoldati, R. Grana, A. Cuoci, T. Faravelli, A.P. Kelley, C.K. Law, Hierarchical and comparative kinetic modeling of laminar flame speeds of hydrocarbon and oxygenated fuels, Prog. Energ. Combust. 38 (2012) 468–501.

[43] C. Xiouris, T.L. Ye, J. Jayachandran, F.N. Egolfopoulos, Laminar flame speeds under engine-relevant conditions: Uncertainty quantification and minimization in spherically expanding flame experiments, Combust. Flame, 163(2016) 270–283.

[44] J.B. Martz, H. Kwak, H.G. Im, G.A. Lavoie, D.N. Assanis, Combustion regime of a reacting front propagating into an auto-igniting mixture, Proc. Combust. Inst. 33 (2011) 3001–3006.

[45] X. Shi, J.Y. Chen, Z. Chen, Numerical study of laminar flame speed of fuel-stratified hydrogen/air flames, Combust. Flame 163 (2016) 394–405.

[46] H. Yu, Z. Chen, End-gas auto-ignition and detonation development in a closed chamber, Combust. Flame 162 (2015) 4102–4111.

[47] J.Y. Pan, G.Q. Shu, P. Zhao, H.Q. Wei, Z. Chen, Interactions of flame propagation, auto-ignition and pressure wave during knocking combustion, Combust. Flame 164 (2016) 319–328.

[48] H.Y. Zhang, E.R. Hawkes, J.H. Chen, S. Kook, A numerical study of the autoignition of dimethyl ether with temperature inhomogeneities, Proc. Combust. Inst. 34 (2013) 803–812.

[49] J.Y. Pan, P. Zhao, C.K. Law, H.Q. Wei, A predictive Livengood–Wu correlation for two-stage ignition, Int. J. Engine Res. 17 (8) (2016) 825–835.